# Quantum phases of attractive matter waves in a toroidal trap

A. Parola,[1] L. Salasnich,[2] R. Rota,[2] and L. Reatto[2]
[1]*Dipartimento di Fisica e Matematica, Università dell'Insubria, Via Valleggio 11, 22100 Como, Italy*
[2]*Dipartimento di Fisica and CNR-INFM, Università di Milano, Via Celoria 16, 20133 Milano, Italy*
(Received 18 April 2005; published 13 December 2005)

Investigating the quantum phase transition in a ring from a uniform attractive Bose-Einstein condensate to a localized bright soliton we find that the soliton undergoes transverse collapse at a critical interaction strength, which depends on the ring dimensions. In addition, we predict the existence of other soliton configurations with many peaks, showing that they have a limited stability domain. Finally, we show that the phase diagram displays several new features when the toroidal trap is set in rotation.

DOI: 10.1103/PhysRevA.72.063612 PACS number(s): 03.75.Kk

## I. INTRODUCTION

Metastable states of Bose Einstein condensates (BECs) made of attractive $^7$Li atoms, namely single and multiple bright soliton configurations, have been observed in two different experiments [1,2]. These metastable bright solitons, which can travel for long distances without dispersion, have been the subject of various theoretical investigations because of their relevance in nonlinear atom optics [3,4]. Repulsive BECs in a quasi-one-dimensional (1D) ring have been produced and studied [5]. The case of an attractive BEC in a ring has not yet been experimentally investigated but appears very interesting. For this system a quantum phase transition from a uniform condensate to a bright soliton. has been predicted by Kavoulakis and by Kanamoto, Saito, and Ueda [6]. This prediction is based on mean-field and beyond mean-field numerical results for a 1D Bose gas with contact interaction and periodic boundary conditions [6]. Later, the same authors have shown that the quantum transition properties of the attractive BEC in a 1D ring are strongly modified if the confining trap is rotating [7].

In this paper we investigate an attractive BEC in a three-dimensional (3D) ring, taking into account transverse variations of the BEC width, showing that the phase diagram of the system reveals peculiar structures. In particular, we prove that, contrary to the simple 1D case, the localized soliton has a limited existence and stability domain, which nevertheless strongly extends the stability domain of the uniform solution. Moreover, we find that the system supports also multipeak solitons, which are energetically unstable but can be dynamically stable. Finally, we analyze the effect of a rotating ring. In this case the multipeak solitons are always energetically and dynamically unstable, while the one-peak soliton is stable in a domain that, for a fixed rotation frequency, critically depends on the system parameters.

## II. TOROIDAL TRAP

We consider a BEC confined in a toroidal potential given by

$$U(\rho,\zeta)=\frac{1}{2}m\omega_\perp^2[(\rho-R_0)^2+\zeta^2], \tag{1}$$

where $\rho$ is the cylindric radial coordinate, $\zeta$ is the cylindric axial coordinate, and $\theta$ is the azimuthal angle. The BEC has transverse harmonic confinement of frequency $\omega_\perp$ and the two characteristic lengths of the toroidal trap are $R_0$ and $a_\perp=[\hbar/(m\omega_\perp)]^{1/2}$. In the remaining part of the paper we use scaled units; time in units of $\omega_\perp^{-1}$, length in units of $a_\perp$, and energy in units of $\hbar\omega_\perp$. To simplify the 3D Gross-Pitaevskii equation (GPE) we impose that the order parameter $\Psi(\rho,\theta,\zeta,t)$ of the Bose condensate is the product of a generic azimuthal function $f(\theta,t)$ and a radial Gaussian function, which has two variational parameters; the width $\sigma(\theta,t)$ and the coordinate $R$ of the center of mass in the radial direction. The trial wave function is given by

$$\Psi(\rho,\theta,\zeta,t)=\frac{f(\theta,t)}{R^{1/2}}\frac{\exp\left(-\frac{(\rho-R)^2+\zeta^2}{2\sigma(\theta,t)^2}\right)}{\pi^{1/2}\sigma(\theta,t)}. \tag{2}$$

We follow a procedure similar to that described in [8] inserting the trial wave function into the GPE Lagrangian density

$$\mathcal{L}=\Psi^*\left[i\frac{\partial}{\partial t}+\frac{1}{2}\nabla^2-U-\frac{1}{2}\Gamma|\Psi|^2\right]\Psi, \tag{3}$$

where $\Gamma=4\pi a_s N/a_\perp$, with $N$ the number of condensed atoms and $a_s<0$ the attractive $s$-wave scattering length. The trapping potential of Eq. (1) has a cusp at the origin, a feature not usually present in experimental traps, but this is expected to have minor effects on physical properties if only a small fraction of the particles are near the origin. For example, if $R/\sigma>3/2$, the fraction of particles belonging to the radial region $[0,R-\sigma]$ is below 1%. In the range $1<R/\sigma<3/2$ the population near the origin is not so small and the results reported below are not fully reliable in this range. We integrate over $\rho$ and $\zeta$ coordinates [9]. In this way, from the Euler-Lagrange equations of the resulting effective Lagrangian density, we get the nonpolynomial Schrödinger equation (NPSE)

$$\left[i\frac{\partial}{\partial t}+\frac{1}{2}\frac{\partial^2}{\partial z^2}-T(n)\right]\psi=0, \tag{4}$$

where $\psi(z,t)=f(\theta,t)/R^{1/2}$ is the azimuthal wave function of the condensate with $z=R\theta$, $n=|\psi|^2$ is the density profile normalized to unity and $T(n)=dW(n)/(dn)$ with $W(n)=n(1-gn)^{1/2}$. The scaled interaction strength $g$ is given by

 

$g=|\Gamma|/(2\pi)=2N|a_s|/a_\perp$. In toroidal geometry the solution $\psi(z,t)$ must obey periodic boundary conditions $\psi(0,t)=\psi(L,t)$ with $L=2\pi R$. Within our variational approach the transverse width $\sigma$ of the BEC is given by

$$\sigma^2=(1-gn)^{1/2}. \tag{5}$$

For $gn\ll 1$ one has $\sigma\simeq 1$, $T(n)\simeq -gn+1$, and the NPSE reduces to the 1D GPE. In addition, we find that the variational parameter $R$ is implicitly given by the equation

$$R-\frac{1}{R}\int_0^{2\pi R}\left|\frac{\partial\psi}{\partial z}\right|^2 dz+\frac{g}{2\sigma^2}\int_0^{2\pi R}|\psi|^4 dz=R_0. \tag{6}$$

This formula shows that the effective radius $R$ of the BEC ring depends on the interaction strength $g$. We have verified that for a static and attractive BEC, the effective radius $R$ decreases very slowly by increasing $g$, while for a repulsive BEC the opposite is true. In practice, because for an attractive BEC the strength $g$ cannot exceed the scaled inverse density $n^{-1}$, the effective radius $R$ is always close to $R_0$. For a uniform BEC, where Eq. (6) becomes $R+g/\{4\pi R^2[1-g/(2\pi R)]^{1/2}\}=R_0$, it is easy to check that the relative difference between $R$ and $R_0$ is typically only a few percent and becomes 10% only near the collapse.

The very good accuracy of the NPSE in approximating the 3D GPE with a transverse harmonic potential has been verified in [8] for both positive and negative scattering length. In the derivation of NPSE one neglects the space and time derivatives of the width $\sigma(z,t)$. By including these terms one gets the coupled equations derived by Kamchatnov and Shchesnovich [10], but it is not clear if these terms give an improvement. We have verified that, according to the 3D GPE, the single-peak bright soliton of an attractive BEC in an infinite cylinder collapses at the critical strength $g_c/2=0.676$ (see also [11]), a value very close to the NPSE prediction $g_c/2=2/3=0.66\bar{6}$ [8].

## III. UNIFORM AND LOCALIZED SOLUTIONS

The NPSE conserves both the norm of the wave function and the total energy $E$ of the configuration. The stationary solutions follow from Eq. (4) by looking for solutions of the form $\psi(z,t)=\phi(z)e^{-i\mu t}$ for some chemical potential $\mu$. The resulting nonlinear eigenvalue equation is the static NPSE. In toroidal geometry, the uniform solution $\phi(z)=1/\sqrt{L}$ is always present for $g<L$, i.e., with density $N/L<a_\perp/(2|a_s|)$, and corresponds to the eigenvalue $\mu=T(1/L)$. In addition, other less trivial profiles may be present. Beyond this limit (i.e., for $g>L$) the attraction is too strong and no regular solution is possible, leaving the BEC collapse as the only possibility. A generic (real) solution $\phi(z)$ of the stationary NPSE may be interpreted as the classical "time" evolution of a fictitious particle moving in a potential $V(\phi)=\mu\phi^2-W(\phi^2)$. As a consequence, the "energy" conservation equation for this motion reads

$$\frac{1}{2}\left(\frac{d\phi}{dz}\right)^2+V(\phi)=\epsilon. \tag{7}$$

According to the values of the two parameters $\mu$ and $\epsilon$ two kinds of "trajectories" may be realized. For $\mu>0$ and $\epsilon>0$ the solution $\phi(z)$ oscillates between a positive and a negative value, thereby crossing zero, while for $\epsilon<0$ the solution $\phi(z)$ remains always positive. In the first case the solutions are named *nodal solitons* while in the second case *nodeless solitons*.

For fixed $g$ and $L$, the two parameters $\mu$ and $\epsilon$ are implicitly determined by the two consistency equations:

$$L=\sqrt{2}N_s\int_{\phi_{min}}^{\phi_{max}} d\phi\frac{1}{\sqrt{\epsilon-V(\phi)}} \tag{8}$$

and

$$1=\sqrt{2}N_s\int_{\phi_{min}}^{\phi_{max}} d\phi\frac{\phi^2}{\sqrt{\epsilon-V(\phi)}}, \tag{9}$$

where $N_s$ is the number of maxima of the soliton, i.e., the number of "periods" of the corresponding orbit, and $\phi_{min}$ ($\phi_{max}$) is the minimum (maximum) value attained by $\phi(z)$ during the periodic oscillation. As customary in Newtonian problems, the extremal values of $\phi$ are implicitly defined by the equation $V(\phi)=\epsilon$ in terms of $\epsilon$ and $\mu$. The first equation comes from the commensurabilty requirement of the solitonic solution, which, after an integer the number of periods must close without discontinuities. The second equation is just the normalization condition of the wave function.

The two consistency equations (8) and (9) have been solved and the domain of existence of soliton solutions of the given topology has been determined in the $(R,g)$ plane. The results are shown in Fig. 1. The numerical analysis shows that two solutions of same symmetry may be present in a portion of the existence domain. For the sake of clarity in Fig. 1 we report the existence domain only for the one-peak soliton ($N_s=1$) and for the two-peak soliton ($N_s=2$). Note that the existence diagram of the 1D GPE is strongly different from that of the NPSE. In fact, as previously stressed, the 1D GPE does not take into account the transverse dynamics and, as a consequence, no collapse of solitonic solutions is predicted by 1D GPE.

## IV. ENERGETIC STABILITY

We now turn to the discussion of the energetic stability [12] of the previously defined solitonic configurations. One can rigorously prove that the energetic stability can be expressed in terms of the eigenvalues $\lambda_l$ of $H\pm nT'$, where

$$H=-\frac{1}{2}\frac{d^2}{dz^2}+T(n)+n\frac{dT(n)}{dn}-\mu \tag{10}$$

and $n(z)$ is the density profile of the stationary solution. The stationary solution $\phi(z)$ is energetically stable only if either of the two conditions is satisfied: (1) all the eigenvalues $\lambda_l$ are non-negative and (2) a single negative eigenvalue $\lambda_0$ is present and $dg/d\mu\leqslant 0$. When we apply this general analysis

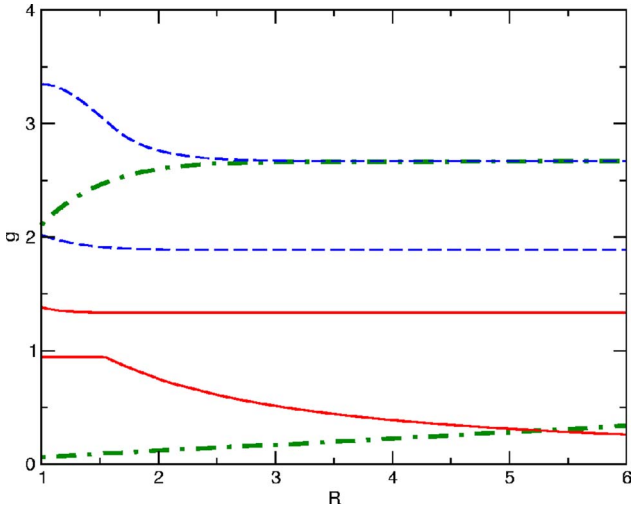


FIG. 1. (Color online) Existence diagram in the $(R,g)$ plane, where $g=2N|a_s|/a_\perp$ is the interaction coupling and $R=L/(2\pi)$ is the azimuthal radius of the ring (in units $a_\perp$). A uniform solution exists for $g<2\pi R$. A one-peak localized nodeless solution exists between the two solid lines. Nodeless two-peak localized solution exists between the two dashed lines. The nodal two-peak localized solution exists between the two dot-dashed lines.

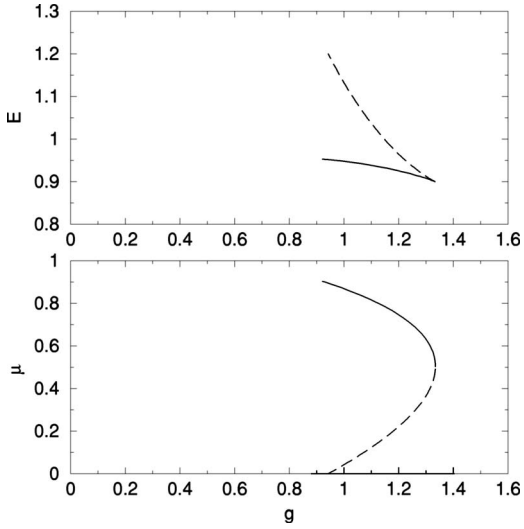


FIG. 2. Energy $E$ and chemical potential $\mu$ of the one-peak solitons as a function of the coupling $g$ for $L=10$. The energetically stable solutions are represented by the solid lines, the unstable solutions are represented by the dashed lines.

to the simple case of the uniform stationary solution in toroidal geometry $\phi(z)=1/\sqrt{L}$ we find that this case satisfies the latter of the two conditions previously stated and the solution is stable until the second eigenvalue gets negative, triggering the instability. The resulting stability condition $(2\pi/L)^2+4nT'\geqslant 0$ explicitly becomes

$$\frac{\pi^2}{gL}\left(1-\frac{g}{L}\right)^{3/2}\geqslant\left(1-\frac{3g}{4L}\right). \tag{11}$$

This formula reduces to $\pi^2/(gL)$ for large $L$ (1D limit), that is precisely the result one finds with the 1D GPE [6]. The stability analysis of the solitonic configurations, however, does not allow for a general analytic solution and the eigenvalue equations of $H\pm nT'$ must be investigated numerically.

The operators $H\pm nT'$ may be numerically diagonalized by introducing a finite mesh in the interval $0\leqslant z<L$ and approximating the differential operator with the corresponding finite difference operator. The two resulting equations then give rise to a matrix eigenvalue problem. The numerical results show the following.

(i) In the regions where the uniform solution satisfies the energetic stability condition $dg/d\mu\leqslant 0$ no other solitonic wave function can be stabilized.

(ii) Only the one peak soliton is energetically stable in a portion of the domain where it is defined.

(iii) When distinct, one peak solutions exist for the same values of $g$ and $L$. The soliton is stable only in the branch corresponding to the lowest energy.

The latter remark is illustrated in the upper panel of Fig. 2, where the energy $E$ of the one-peak solution is shown as a function of $g$ for $L=10$. It is also interesting to plot the chemical potential $\mu$ versus $g$ in the stable and unstable branch. The case of $L=10$ previously analyzed is shown in the lower panel of Fig. 2, where it appears that the onset of instability corresponds to an extremum of the coupling constant $g$ as a function of the chemical potential. In fact, this immediately follows from the previous analysis which led to $dg/d\mu\leqslant 0$. If $H+nT'$ admits a single negative eigenvalue, $dg/d\mu=0$ signals the onset of the instability.

The energetic stability region of stationary solutions of the NPSE in a ring is shown in the top panel ($\Omega=0$) of Fig. 3. Below the solid curve the uniform solution is energetically stable. The one-peak soliton, which exists between the two dashed curves, is energetically stable in the domain limited by the solid and the upper dashed line. In the remaining regions of the phase diagrams no energetically stable stationary solution is present and the BEC is expected to collapse. Note that for large $R=L/(2\pi)$ the upper dashed line tends to $g=4/3$, that is the formula one finds for the collapse of a bright soliton in a infinite cylinder [see Salasnich *et al.* [3(b)]]. It is not difficult to show that with a large $R$ the existence domain of a $N_s$ peak bright soliton is instead given by

$$0<g<\frac{4}{3}N_s. \tag{12}$$

See, for instance, the existence domain of the two-peak solitons shown in Fig. 1. As previously stressed, upper bounds do not exist within the 1D GPE approach; the collapse of single and multiple bright solitons is due to the transverse dynamics of the condensate.

In the other panels of Fig. 3 the effect of a rotating toroidal trap on the attractive BEC is shown. The analysis is developed by observing that one has to include the centrifugal operator

$$-\Omega\hat{M}_\theta=i\Omega\frac{L}{2\pi}\frac{\partial}{\partial z} \tag{13}$$

into Eq. (4), where $\Omega$ is the rotation frequency (in units of the frequency $\omega_\perp$ of the harmonic transverse confinement)

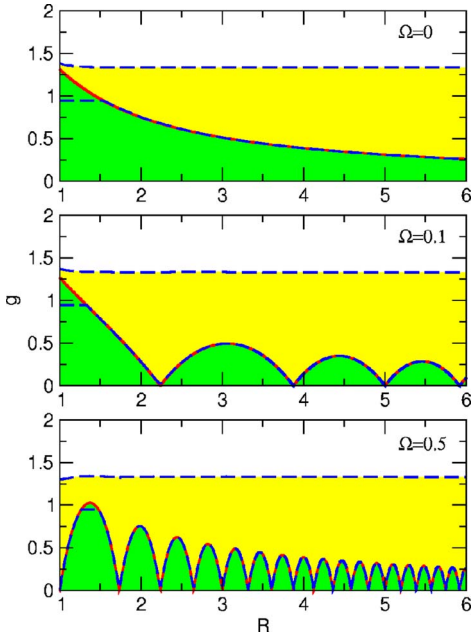


FIG. 3. (Color online) Attractive BEC in a ring rotating with frequency $\Omega$. Energetic-stability diagram in the plane $(R,g)$. The uniform solution is the ground state only below the solid line. The one-peak localized solution exists between the two dashed lines but it is the ground state only between the solid line and the upper dashed line. Note that for almost all $R=L/(2\pi)$ the solid curve is superimposed to the lowest dashed curve. Only for $1<R<1.5$ is the lowest dashed line below the solid line.

and $\hat{M}_\theta$ is the azimuthal angular momentum. As shown in Ref. [7] by using the 1D GPE, the uniform state of the attractive BEC is superfluid, i.e., it exists a critical frequency $\Omega_c$ below which the uniform state remains stationary, and only above this critical frequency the uniform state rotates. In general, the stationary uniform solution is thus given by $\psi(z)=e^{i2\pi zj/L}/\sqrt{L}$, where the integer number $j$ is a function of $\Omega$ and $L$, namely,

$$j(\Omega,L)=\mathrm{int}\left[\frac{\Omega L^2}{4\pi^2}+\frac{1}{2}\right], \tag{14}$$

with int$[x]$ the maximum integer that does not exceed $x$. The localized soliton solution has a different behavior; its angular momentum is not quantized [7] and this means that the quantum phase transition from the uniform to the localized state suppresses the superfluidity of the system [7]. Setting $\psi(z)=\phi(z)e^{i\alpha(z)}$, where both $\phi(z)$ and $\alpha(z)$ are real, from the stationary NPSE with the centrifugal operator of Eq. (13) one finds

$$\frac{d\alpha}{dz}=\Omega\frac{L}{2\pi}+\frac{c}{\phi^2}, \tag{15}$$

where the constant $c$ is given by the equation

$$\Omega R^2+\frac{c}{2\pi}\int_0^L\frac{dz}{\phi(z)^2}=j. \tag{16}$$

In addition, the function $\phi(z)$ is obtained from the two consistency Eqs. (8) and (9) with $V(\phi)$ now given by

$$V(\phi)=\mu+\frac{1}{2}\left(\frac{\Omega L}{2\pi}\right)^2-W(\phi)+\frac{c^2}{2\phi^2}, \tag{17}$$

where $W(\phi)=\phi^2(1-g\phi^2)^{1/2}$.

Following the previous analysis one finds that the energetic stability condition reads

$$1-4\left(\frac{\Omega L^2}{4\pi^2}-j(\Omega,L)\right)^2\leqslant\frac{gL}{\pi^2}\frac{\left(1-\frac{3g}{4L}\right)}{\left(1-\frac{g}{L}\right)^{3/2}}. \tag{18}$$

In the 1D limit of large $L$ the previous formula gives $1-4[(\Omega L^2/4\pi^2)-j(\Omega,L)]^2\geqslant gL/\pi^2$, that is, the results found in Ref. [7]. Figure 3 shows the energetic stability diagram in the plane $(R,g)$ for two nonzero values of the rotating frequency $\Omega$. Below the solid line the stability condition holds and the uniform state is energetically stable. The periodic structure for $\Omega\neq 0$ is a consequence of the periodic quantization of the angular momentum $j(\Omega,L)$. In particular, for a fixed $\Omega$, the solid line touches the horizontal axis $g=0$ for discrete values of $R=L/(2\pi)$, which correspond to jumps in the quantum number $j$.

The one-peak solitonic solution exists between the two dashed lines and it is energetically stable between the solid line and the upper dashed line. Interestingly, Fig. 3 shows that for large $R$ the lower dashed line and the solid line practically coincide. As in the nonrotating case, we find that also for $\Omega\neq 0$ solutions with more than one peak are not energetically stable.

In Fig. 4 we plot the angular momentum $M_\theta$ and the azimuthal width $\Sigma$ of the rotating one-peak bright soliton. The figure shows that the angular momentum is not quantized. It approaches the value $M_\theta=\Omega R^2$ of a "classical particle" for $g$ close to the collapse ($g\simeq 4/3$), but it becomes quantized, i.e., $M_\theta=j$, where $j$ depends on $\Omega$ and $R$, for the small value of $g$ that gives the transition to the uniform solution. Obviously, when the angular momentum becomes quantized the width $\Sigma$ of the bright soliton coincides with that of the uniform solution. Figure 4 also shows that the width $\Sigma$ is independent on the ring radius $R$ as the bright soliton is close to the collapse; in this case $g\simeq 4/3$ and $\Sigma\simeq 0.85$.

## V. DYNAMICAL STABILITY

It is important to stress that energetic stability implies dynamical stability but the converse is not true [12]. In order to investigate the dynamical stability of stationary solutions in the ring one can solve the Bogoliubov–de Gennes (BdG) equations which give the elementary excitations $\epsilon_l$ $(l=1,2,3,\ldots)$ of the system; the appearence of a complex excitation signals dynamical instability while a negative excitation implies energetic instability [12]. For the uniform solution $\psi(z)=e^{i2\pi zj/L}/\sqrt{L}$ one finds

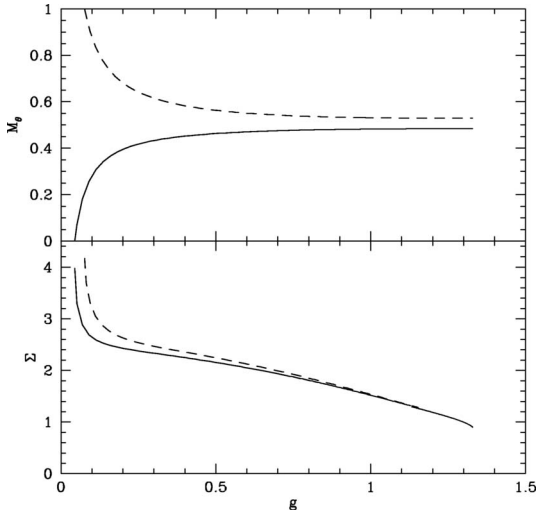


FIG. 4. Angular momentum $M_\theta=\langle\hat{M}_\theta\rangle$ and azimuthal width $\Sigma=\langle z^2\rangle^{1/2}$ of the one-peak soliton as a function of the coupling $g$ for $\Omega=0.1$ and two values of $R$, $R=2.2$ (solid line) and $R=2.3$ (dashed line).

$$\epsilon_l=-\left(\Omega-\frac{4\pi^2}{L^2}j(\Omega,L)\right)l+\frac{1}{2}\left\{\left(\frac{2\pi l}{L}\right)^2\left[\left(\frac{2\pi l}{L}\right)^2-\frac{4g}{L}\frac{\left(1+\frac{3g}{4L}\right)}{\left(1-\frac{g}{L}\right)^{3/2}}\right]\right\}^{1/2}. \quad (19)$$

This result confirms that the uniform solution is energetically stable if the previously written stability condition is satisfied; moreover it shows that the dynamical stability of the uniform solution is independent on $\Omega$. For localized solutions the BdG equations are computationally rather demanding. For this reason we have analyzed the dynamical stability by numerically solving the time-dependent NPSE taking as an initial condition the stationary localized solution $\phi(z)$ with a very weak perturbation.

In Fig. 5 we plot the density profile $\rho(z)=|\phi(z)|^2$ of the one-peak and the nodal two-peak solutions, choosing $L=15$, $g=1$, and two values of $\Omega$. In addition, we plot the time evolution of the mean squared width $\langle z^2\rangle-\langle z\rangle^2$. Its behavior reveals that these solitonic solutions are dynamically stable. We have investigated the dynamical stability for various initial conditions. For $\Omega=0$ we have found that (i) the one-peak soliton is dynamically stable where it exists; (ii) the nodal two-peak soliton is dynamically stable in the plane $(R,g)$ only below the upper curve of existence of the one-peak soliton; and (iii) the nodeless two-peak soliton is dynamically unstable. Similar results are found for solitonic solutions with a larger number $N_s$ of peaks.

The case $\Omega\neq 0$ leads to similar results, keeping in mind, however, that nodal solitons do not exist under rotation. For high rotational frequencies, namely when $\Omega$ approaches the

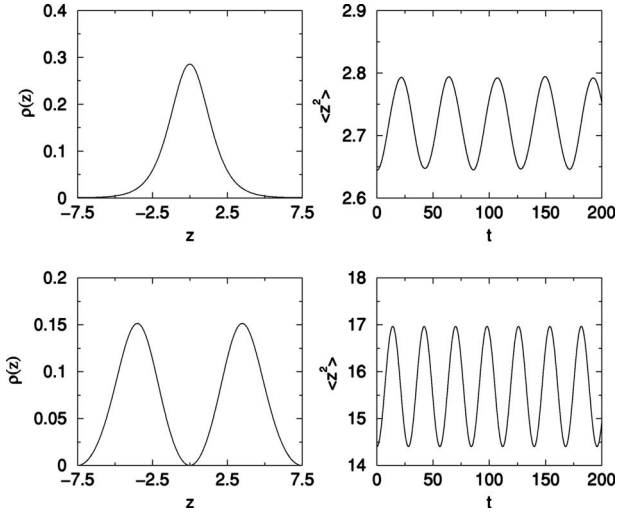


FIG. 5. Left panels show the density profile $\rho(z)$ of the solitonic solutions. Right panels show the time-dependence of the mean squared widths $\langle z^2\rangle-\langle z\rangle^2$ for the weakly perturbed solitonic solutions. Ring axial lenght: $L=15$. Interaction strength: $g=1$. Rotational frequency: $\Omega=0$.

frequency of transverse harmonic confinement (that is 1 in our units), the effect of the centrifugal force on the transverse dynamics becomes relevant. For a given angular momentum $j\simeq R^2\Omega$, the centrifugal force increases the effective radius $R$ of the BEC ring. For a rotating and uniform ideal BEC one easily finds from Eq. (6) that $R=R_0/(1-\Omega^2)$. This formula holds also for an azimuthally localized ideal BEC. At the critical frequency $\Omega=1$ the radius $R$ diverges and this means that the Bose condensate is no longer confined. As in the nonrotating case, an investigation of Eq. (6) shows the effect of the interaction strength $g$ on the effective radius $R$ is negligible for an attractive BEC.

## VI. CONCLUSIONS

We have predicted quantum phases for an attractive Bose condensate in a ring. Our results can be experimentally tested with the optical and magnetic traps developed [5,13], where a time-dependent stirring potential can be used to set the system into rotation. For instance, by choosing $10^3$ $^7$Li atoms ($a_s=-1.4$ nm) in a toroidal trap with $L\simeq 25$ $\mu$m and $a_\perp\simeq 3$ $\mu$m, a sequence of transitions between the uniform state and solitonic configurations takes place when the stirring frequency $\Omega$ is varied between 0 and 1 kHz. These experiments will open the way to the observation of amazing quantum phenomena like solitonic condensate without superfluidity and the dynamically induced phase transition from uniform to localized states.

## ACKNOWLEDGMENTS

The authors thank F. Dalfovo, A. Recati, S. Stringari, and C. Tozzo for useful suggestions.

[1] K. E. Strecker *et al.*, Nature **417**, 150 (2002).
[2] L. Khaykovich *et al.*, Science **296**, 1290 (2002).
[3] (a) U. Al Khawaja, H. T. C. Stoof, R. G. Hulet, K. E. Strecker, and G. B. Partridge, Phys. Rev. Lett. **89**, 200404 (2002); (b) L. Salasnich, A. Parola, and L. Reatto, Phys. Rev. A **66**, 043603 (2002); (c) L. Salasnich, A. Parola, and L. Reatto, Phys. Rev. Lett. **91**, 080405 (2003); (d) L. D. Carr and J. Brand, *ibid.* **92**, 040401 (2004).
[4] L. D. Carr and Y. Castin, Phys. Rev. A **66**, 063602 (2002); L. Salasnich, *ibid.* **70**, 053617 (2004).
[5] S. Gupta, K. W. Murch, K. L. Moore, T. P. Purdy, and D. M. Stamper-Kurn, Phys. Rev. Lett. **95**, 143201 (2005).
[6] G. M. Kavoulakis, Phys. Rev. A **67**, 011601(R) (2003); R. Kanamoto, H. Saito, and M. Ueda, *ibid.* **67**, 013608 (2003).
[7] R. Kanamoto, H. Saito, and M. Ueda, Phys. Rev. A **68**, 043619 (2003); G. M. Kavoulakis, *ibid.* **69**, 023613 (2004).
[8] L. Salasnich, Laser Phys. **12**, 198 (2002); L. Salasnich, A. Parola, and L. Reatto, Phys. Rev. A **65**, 043614 (2002).
[9] The small population near the origin allows us to replace the integration of the variable $\eta=\rho-R$ in the range $[-R,+\infty]$ by $[-\infty,+\infty]$.
[10] A. M. Kamchatnov and V. S. Shchesnovich, Phys. Rev. A **70**, 023604 (2004).
[11] A. Gammal, L. Tomio, T. Frederico, Phys. Rev. A **66**, 043619 (2002).
[12] Y. Castin, in *Coherent Atomic Matter Waves*, edited by R. Kaiser, C. Westbrook, and F. David, Lecture Notes of Les Houches Summer School (EDP Sciences and Springer-Verlag, Berlin, 2001), pp. 1–136.
[13] J. A. Sauer, M. D. Barrett, and M. S. Chapman, Phys. Rev. Lett. **87**, 270401 (2001); A. Kasper *et al.*, J. Opt. B: Quantum Semiclassical Opt. **5**, S143 (2003); A. Hopkins, B. Lev, and H. Mabuchi, Phys. Rev. A **70**, 053616 (2004).